24th COBEM - 2017

24th ABCM International Congress of Mechanical Engineering
December 3-8, 2017, Curitiba, PR, Brazil

COBEM-2017- 0592
TWO-DIMENSIONAL ULTRASOUND TRANSDUCER ARRAY FOR ACOUSTIC RADIATION FORCE IMPULSE IMAGING

Djalma Simões dos Santos
Fernando Mitsuyama Cardoso
Sergio Shiguemi Furuie
School of Engineering, University of São Paulo, Brazil
djalma.simoes@usp.br

Abstract. *Acoustic radiation force impulse (ARFI) imaging is a medical modality that uses a focused ultrasound transducer to generate acoustic radiation force in soft tissues. This is a very promising method because it enables to quantitatively assess mechanical properties of soft tissues. The aim of this work is to design a 2D ultrasound transducer array for ARFI excitation with high efficiency. We proposed a transducer array configuration that is capable of reducing: 1) the number of channels of the ultrasound system; and 2) the large electrical impedance mismatch between the transducer and the voltage source circuitry. The performance of the fabricated transducer was compared to a typical transducer and the results showed a high power transfer efficiency, broad bandwidth and minimum insertion loss, determining optimum parameters for the design of 2D ultrasound transducer arrays used in ARFI imaging.*

Keywords: *2D array, ultrasound, transducer, ARFI imaging, elastography*

1. INTRODUCTION

Acoustic radiation force impulse (ARFI) imaging has received much attention of several groups due to its ability to assess mechanical properties of soft tissues in a non-invasive way (Doherty *et al.*, 2013). ARFI methods use a high-energy focused ultrasound transducer to generate acoustic radiation force and induce localized displacements in soft tissues. Monitoring the response of tissue displacements – in terms of shear wave propagation speed – enables us to quantitatively estimate the stiffness of a region (Nightingale, 2012). Detailed review of ARFI imaging can be found in the texts by Doherty *et al*. (2013), Sarvazyan *et al*. (2012), Ophir *et al*. (1996), and Sarvazyan *et al*. (1995). Unfortunately, the use of ARFI methods are limited to regions no deeper than 10 cm because of risks associated to the great energy concentration nearby the transducer surface – this hinders the application of ARFI in obese patients or deep regions covered by a fat layer, for instance (DeWall, 2013; Benson & Fan, 2012).

We have previously reported – by numerical simulation – the feasibility of ARFI imaging in regions deeper than 10 cm by using a two-dimensional (2D) ultrasound transducer array with a large aperture, which prevents a great energy concentration near the transducer surface (Cardoso *et al.*, 2016). A 2D ultrasound transducer array offers the potential for producing symmetrically focused ultrasound beam as well as steering the focused beam throughout a three-dimensional (3D) volume. However, the development of a 2D array transducer is inherently difficult due to the requirement of a large number of elements with a very small cross-sectional area. Consequently, the electrical impedance of each element is much greater than the corresponding impedance of the voltage source circuitry, resulting in a very poor transmit efficiency (Turnbull and Foster, 1991; Turnbull and Foster, 1992; Goldberg and Smith, 1994). Although this is a crucial factor when developing transducers for ARFI excitation, little attention has been given to it in the literature.

The present paper reports the design of a 128-element 2D array transducer with good performance for ARFI applications. We propose a transducer array arrangement that takes advantage of its geometry to both reduce: 1) the large electrical impedance mismatch between the transducer and the voltage source circuitry; and 2) the number of channels – of the ultrasound system – needed to drive the array elements. This arrangement combines the parallel connection of symmetrical array elements followed by the electrical impedance matching with inductor network. The performance of the fabricated transducer was compared to a typical transducer and the results showed a high transmit efficiency, broad bandwidth and minimum insertion loss, determining optimum parameters for 2D array transducer design used in ARFI imaging.

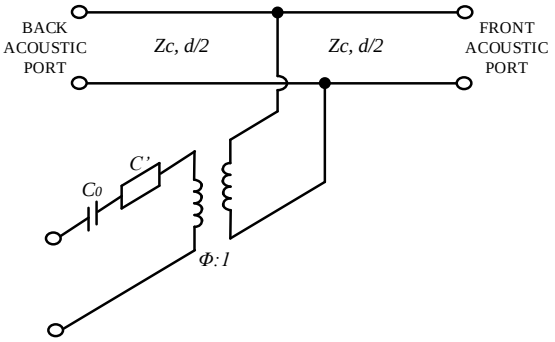

Figure 1. Transmission-line model of a piezoelectric transducer.

2. THEORY

2.1 Transducer equivalent circuits

Numerous sophisticated equivalent circuits have been proposed to model the electrical and mechanical characteristics of ultrasound transducers. The usefulness of the equivalent circuit approach is based on its ability to predict the frequency-dependent electrical impedance and the transmitted and received ultrasound waveforms for a specific transducer (Hunt *et al.*, 1983). The simplest construction of an ultrasonic transducer is a parallel-plate of piezoelectric material with electrodes for connection such as a capacitor structure (Zhou *et al*., 2014; Szabo, 2004). At frequencies away from resonance, the clamped capacitance C_0 of a transducer is given by:

$$C_0 = \varepsilon^S \frac{A}{d} \tag{1}$$

where ε^S is the clamped dielectric constant, A is the cross-sectional area of the transducer and d is the thickness of the piezoelectric material (Bronzino, 2000). A particularly useful equivalent circuit was proposed by Krimholtz, Leedom, and Matthaei (1970), which is referred to as the KLM model. In this model, illustrated in Fig. 1, the transducer is treated as a three-port network connected to the center of an acoustic transmission line, with two ports being mechanical ports representing the front and back surfaces of the piezoelectric crystal and one being an electrical port representing the electrical connection of the piezoelectric material to the electrical generator (Kino, 1987; Shung & Zipparo, 1996). The roles of the electrical and mechanical ports are clearly distinguished, and the electrical input impedance for an arbitrary acoustic load can easily be calculated (or vice versa). The transmission line is driven by a perfect transformer with a frequency-dependent turns ratio $\phi:1$, where

$$\phi = k_T \left(\frac{\pi}{\omega_0 C_0 Z_C} \right)^{\frac{1}{2}} si\,nc\left(\frac{\omega}{2\omega_0} \right) \tag{2}$$

with $si\,nc(x) = \sin(\pi x)/\pi x$. The center frequency of the transducer is ω_0, and Z_C is the acoustic impedance of the piezoelectric material (Szabo, 2004; Hunt, et al., 1983). There is an additional capacitance C' in series with the transformer, however, as $|C'| \gg |C_0|$, it only has a minor influence on the operation of the transducer (Desilets *et al.*, 1978).

The complex electrical impedance Z of a piezoelectric transducer is

$$Z = R_a + jX = R_a + j\frac{1}{\omega C_0} \tag{3}$$

where X and R_a are the imaginary (reactance) and real (radiation resistance) components of the electrical impedance, respectively (Hunt *et al.*, 1983). At resonance, the equivalent circuit for a transmitting transducer irradiating into a medium can be represented by two-port networks consisting of a capacitor and a resistor either in series or in parallel (Kino, 1987). Two important values of the electrical impedance module are easily calculated by using this model: the radiation resistance in series R_a, which is a local minimum point of the impedance; and the radiation resistance in parallel R_m, which is a local maximum of the impedance (Hunt *et al.*, 1983).They are given by:

$$R_a = \frac{4k_T^2}{\pi\omega_0 C_0}\left(\frac{Z_C}{Z_R + Z_L}\right) \tag{4}$$

$$R_m = \frac{\pi}{4k_T^2\omega_1 C_0}\left(\frac{Z_R + Z_L}{Z_C}\right) \tag{5}$$

where ω_0 is the series (resonance) frequency, ω_1 is the parallel (anti-resonance) frequency, k_T is the electromechanical coupling coefficient of the piezoelectric material, Z_C is the acoustic impedance of the piezoelectric material, Z_R is the acoustic impedance of the transducer backing, and Z_L is the acoustic impedance of the load medium (soft tissue or water).

For the case where the cross-sectional area A of the transducer element is very small – commonly in 2D transducers – the assumptions presented from (1) to (5) imply that the small size of the element results in a small clamped capacitance C_0 and, consequently, a large electrical impedance Z near resonance (Goldberg & Smith, 1994). It brings a particular challenge that shall be considered when designing a 2D array transducer: the transmit efficiency, which is a very important factor for ARFI excitation.

2.2 Power transfer efficiency

To outline the effect of a significantly large impedance of the transducer in the power transfer efficiency, consider the block diagram shown in Fig. 2, which illustrates the electrical loads for a single array element connected to an ultrasound system. Poor transmit efficiency is a consequence of the enormous impedance mismatch between a typical 50 Ω transmit circuitry and the impedance of the array element – about three orders of magnitude larger.

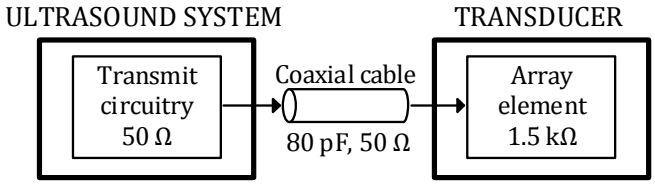

Figure 2. A single transducer array element connected to an ultrasound system.

The simplified circuit in Fig. 3 shows a transmit circuitry formed by voltage source V_{in}, whose impedance is R_0, and a transducer at its resonant frequency ω_0 with clamped capacitance C_0 and real impedance R_a.

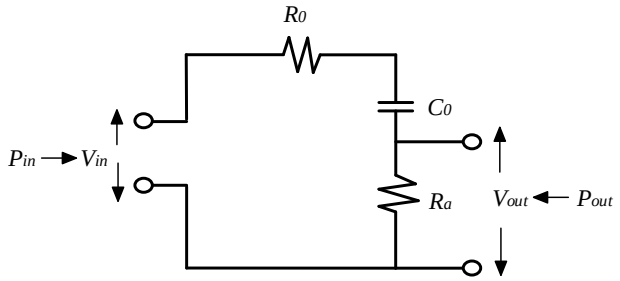

Figure 3. Equivalent circuit of a piezoelectric transducer at its resonant frequency.

According to Kino (1987), the maximum power available from the voltage source is

$$P_{in} = \frac{V_{in}^2}{8R_0} \tag{6}$$

The power delivered to the transducer is proportional to the power dissipated in R_a, which is

$$P_{out} = \frac{V_{out}^2}{2R_a} = \frac{V_{in}^2 R_a}{2[(R_0 + R_a)^2 + (1/\omega_0 C_0)^2]} \tag{7}$$

where $V_{out} = V_{in} R_a / \left(R_0 + R_a + j1/\omega_0 C_0\right)$. Hence, the power efficiency η is

$$\eta = \frac{P_{out}}{P_{in}} = \frac{4R_0 R_a}{\left(R_0 + R_a\right)^2 + \left(1/\omega_0 C_0\right)^2} \tag{8}$$

For a fixed-source impedance, the maximum power efficiency is obtained by taking the derivative of Eq. (8) with respect to R_a and setting it to zero. Hence, η is maximum when $R_0 = \left[R_a^2 + (1/\omega_0 C_0)^2\right]^{1/2}$ and the maximum power transfer occurs when the complex electrical impedance of the transducer is entirely real and the radiation resistance equals the transmit circuitry resistance, *i.e.*, $R_a = R_0$ (Desilets *et al.*, 1978; Bronzino, 2000; Kino, 1987).

Researchers have investigated methods to improve the transmit efficiency of transducers by: 1) using transformers with adjustable turn ratio so that the element electrical impedance matches the voltage source impedance; 2) using electrical network of inductors to lower the imaginary component of the electrical impedance; 3) using multilayers of piezoelectric materials to increase the clamped capacitance of the array element and reduce its electrical impedance (Bronzino, 2000; Goldberg & Smith, 1994). The use of transformers is very difficult to implement in the large quantities required for a 2D transducer array due to space limitations. Inductor networks have successfully been used in transducers for many years, however, an inductor network may significantly narrow the bandwidth of a very tiny element – generally, a more sophisticated tuning network is desirable for broader bandwidth operation (Desilets *et al.*, 1978). Finally, the use of multilayer piezoelectric material can effectively improve the transducer transmit sensitivity by increasing the clamped capacitance of the layer structure. Nevertheless, the fabrication of multilayers involves thick film technologies that become very complex for a 2D array transducer (Goldberg & Smith, 1994).

3. METHODS

3.1 Design and fabrication

In this study, the 2D transducer array introduced by Cardoso *et al.* (2016) with a center frequency of 800 kHz was fabricated using lead-zirconate-titanate (Pz37) ceramic that is commercially available (Ferroperm Piezoceramics A/S). Since transducer arrays for ARFI excitation are constantly focused, we considered an array arrangement that takes advantage of its symmetry with the intention of minimizing the number of channels necessary to drive the array elements. This arrangement was also beneficial to reduce the electrical impedance of the transducer, which shall be soon explained.

For the sake of simplicity, consider the linear transducer array connected to an ultrasound system shown in Fig. 4(a). The transducer consists of *N* elements driven by *N* channels programmed with *N* time delays to enable us to focus and steer the beam at that given focal point with a focal length *r* and a focal angle θ (in polar coordinates). Note that, when the transducer array is focused at the center of its aperture, the delays applied on its symmetrical elements – in relation to the center of the aperture – are equivalent to each other, as depicted in Fig. 4(b). The same effect is obtained if pairs of symmetrical elements are electrically connected in parallel. In this situation, the number of necessary channels to drive the linear transducer array can be reduced by: 1) *N/2* if *N* is an even number; or 2) *N/2+1* if *N* is odd. As a consequence of this reduction, a degree of freedom of the ultrasound beam is eliminated. In other words, the linear transducer will be capable of varying its focal length, but will be unable to vary its focal angle, making the ultrasound beam remain constantly normal to the transducer surface.

In the case of 2D transducer array, symmetrical element pairs can be formed in relation to the center of the aperture in the lateral and elevational directions, resulting in the cancellation of the azimuth and elevation degrees of freedom, respectively (in spherical coordinates). On this basis, we designed a 2D transducer array formed by 128 elements in a 13×10 geometry (with two inactive elements) and applied the reduction of channels in one direction. The main design parameters and geometry of the proposed transducer are schematically shown in Fig. 5.

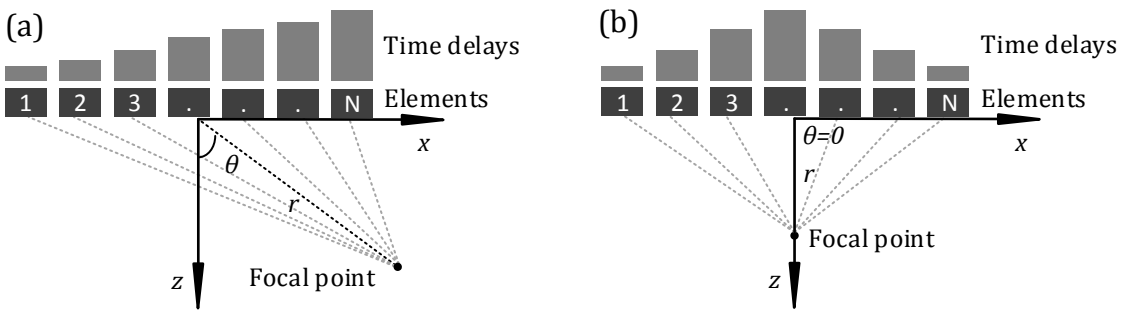

Figure 4. Focalization of a linear array. (a) Steered off axis. (b) On axis.

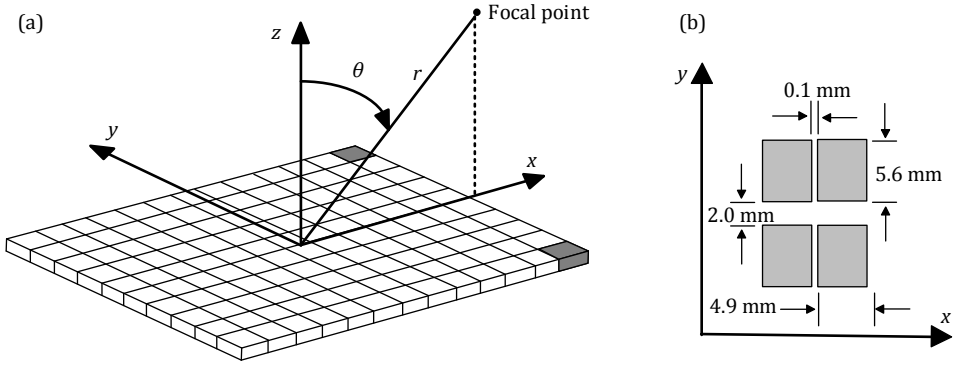

Figure 5. Transducer geometry and coordinate system. (a) Each element pair is symmetrical in relation to the *x* axis and is driven by a single channel. (b) Element and kerf dimensions.

The fabrication of the proposed transducer starts from a piezoelectric ceramic plate consisting of lead-zirconate-titanate (Pz37) with dimensions of 80×80×1.43 mm. The first step was to determine the direction of the piezoelectric ceramic polarization and identify its ground face to optimize cut and construction. After properly cleaned, the piezoelectric ceramic was affixed on a phenolite board, which was used as a sacrificial layer, and glued together on the smooth surface of a glass plate to eliminate any movement and enhance flatness during cut. Then, the sandwich formed by the Pz37 ceramic, phenolite board and glass plate, from the top to the bottom, respectively, was placed on the vacuum chuck table of an automatic dicing saw (DAD322, DISCO Corporation) and two sets of perpendicular scribes – used as reference for cutting – were made with a 0.1 mm wide-blade.

With the ground face of the piezoelectric ceramic on the bottom and the positive one on the top, thirteen parallel sets of non-through cuts were made. The distance between cuts was 4.9 mm and the ground face of the ceramic remained intact. Later on, the ceramic was cut through in ten parallel cuts – of 5.6 mm distance – in a perpendicular direction to the previous ones, resulting in ten separated piezoelectric ceramic strips with thirteen elements of $4.9 \times 5.6 \times 1.43$ mm and 0.1 mm kerf – blade thickness – between them. All elements of each ceramic strip share a common bottom, *i.e.*, common ground, to avoid soldering and to ease the alignment and mounting of the array.

After the cutting process, the strips of Pz37 ceramic were properly arranged to compound the 2D array. Electrode boards were placed between the strips to both give mechanical support and to facilitate the electrical contact of the elements. The thickness of the electrode boards is 2 mm, which is the kerf in the *y* direction.

The electrical connections between the array elements and cables were carried out in three steps: firstly, wires were soldered to connect the elements to the electrode board; secondly, all symmetrical elements in relation to the *x* axis were electrically connected with wires in order to receive the same signal from a single channel, as previously explained.

We kept the transducer air-backed to allow as much energy irradiated into the forward direction as possible (Shung & Zipparo, 1996). To maximize the acoustic transmission, a matching layer of $\lambda/4$ thickness made of epoxy and alumina powder was constructed (λ= wavelength in the matching layer material). The acoustic impedance of the matching layer Z_m was selected to be $Z_m = (Z_C Z_L)^{1/2}$, where Z_C and Z_L are the acoustic impedances of piezoelectric ceramic and the loading medium, respectively (Zhou *et al.*, 2014; Kino, 1987; Kinsler and Frey, 1962; Oliveira, 2015).

The transducer housing consists of four walls and one top lid made of phenolite board, which were posteriorly shielded with an electrically conductive adhesive tape. Finally, a 1.5 m coaxial cable was connected to the electrodes and a plastic cable clamp was used to secure the coaxial cable into the housing.

3.2 Electrical impedance analysis

Besides the reduction of channels needed to drive the array elements, the parallel connection of symmetrical element pairs – described in the previous sections – plays an important role in reducing the electrical impedance of each element of the fabricated transducer. To understand the performance of this arrangement, consider the single element depicted in Fig. 6(a) and the two parallelly connected elements with equivalent overall dimensions in Fig. 6(b). The parallel connection of a symmetrical element pair in relation to the center of aperture shall be herein referred simply as element pair. The theoretical clamped capacitance of a single element is given by Eq. (1). Nevertheless, when N piezoelectric elements are connected in parallel, the total cross-sectional area of this association A_T is the sum of each element area. Hence, the total clamped capacitance C_N of the configuration is increased by a factor N:

$$C_N = \frac{\varepsilon^S A_T}{d} = N \frac{\varepsilon^S A}{d} = N C_0 \tag{9}$$

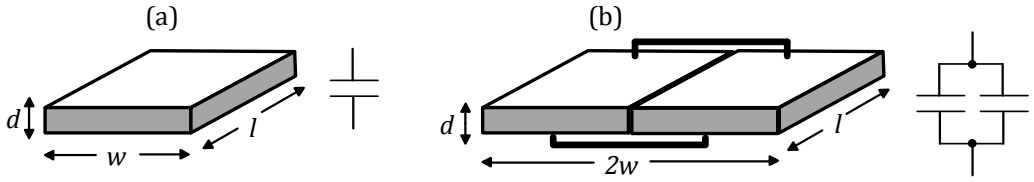

Figure 6. Overall dimensions and equivalent configuration. (a) A single piezoelectric element. (b) Parallelly connected element pair.

Thus, when array elements are electrically connected in parallel, the resultant association has an increase of clamped capacitance and a decrease of electrical impedance if compared to a single element. For *N=2*, the theoretical clamped capacitance of a single array element of the fabricated transducer is 195.4 pF. For an element pair, this value is 390.8 pF.

Although the parallel connection of symmetrical elements reduces the magnitude of the electrical impedance of piezoelectric elements, it does not alter its complex characteristic – in other words, the electrical impedance is not real over the passband. In order to eliminate the imaginary component of the electrical impedance at resonance and enhance the power transferred to the transducer, an electrical impedance matching is required. This was done by the insertion of an electrical network of inductors, which is responsible to tune out the capacitive reactance $X=j1/\omega_0 C_0$ and maintain the element electrical impedance exclusive real. A series tuning inductive reactance $X_L=\omega_0 L$ was chosen so that it equals the capacitive reactance $X_L = X$.

Experimental measurements of the electrical impedance of the fabricated transducer were performed at all stages by using a precision impedance analyzer (4294A, Agilent Technologies).

3.3 Numerical Simulations and experimental setup

To provide a way of evaluating the electrical features of the fabricated transducer beforehand, a KLM model program was developed in MATLAB (The Mathworks Inc.) and the results were compared with experimental impedance measurements. Table 1 lists the main parameters inserted in the KLM model simulation.

The acoustic field of the designed transducer was simulated in the program FOCUS Ultrasound Simulator (Michigan State University) using one cycle tone-burst as excitation function. At a late stage, an experimental setup formed by water tank, X-Y-Z manipulator, PVDF needle hydrophone (diameter of 1 mm) and data acquisition system was used to measure the radiation pattern of the fabricated transducer. Simulated and experimental results were compared (unfortunately, it was not possible to simultaneously drive all 128 array elements of the fabricated transducer due to a failure in our ultrasound system. Instead, a single element and element pair were driven and compared with simulations. Future work should therefore include experimental measurements of focusing and steering properties of the designed transducer).

4. RESULTS AND DISCUSSION

As shown in Fig. 7(a), the electrical impedance magnitude of a single element at series and parallel resonance are 900 Ω and 1200 Ω, respectively. Experimental measurements of the impedance magnitude are in relatively good agreement with the KLM model simulation at regions near the resonance frequency. Discrepancies found at some frequencies may be attributed to the accuracy of the model, which neglects external variables apart from the piezoelectric element itself, such as wires, solders and connectors. After the parallel connection of element pairs, the electrical impedance was reduced by half, as can be seen in Fig. 7(b). However, the element pair characteristics are still essentially capacitive, *i.e.*, no changes occurred in the impedance phase spectrum.

By separating the resistive and reactive components of the electrical impedance at the resonance frequency, it was observed that the element pairs displayed an averaged resistance of approximately 130 Ω and capacitive reactance of 520 Ω. Hence, a series inductor L of 100 µH was used to make $X_L = X$ and cancel the imaginary parts of the electrical impedance. Figure 8 compares the element pair impedance before and after the insertion of a series tuning inductor.

Table 1. Main parameters entered into the KLM model simulation.

Material	Sound speed c (m/s)	Acoustic impedance (MRayls)	Thickness (mm)	Relative dielectric permittivity $\varepsilon^S/\varepsilon_0$	Coupling factor thickness k_t
Water	1540	1.5	infinite	–	–
Alumina epoxy (matching layer)	2823	5.26	λ/4=0.7	–	–
Pz37	2727	18	1.43	1150	0.52
Air-backed (backing layer)	330	0.0004	infinite	–	–

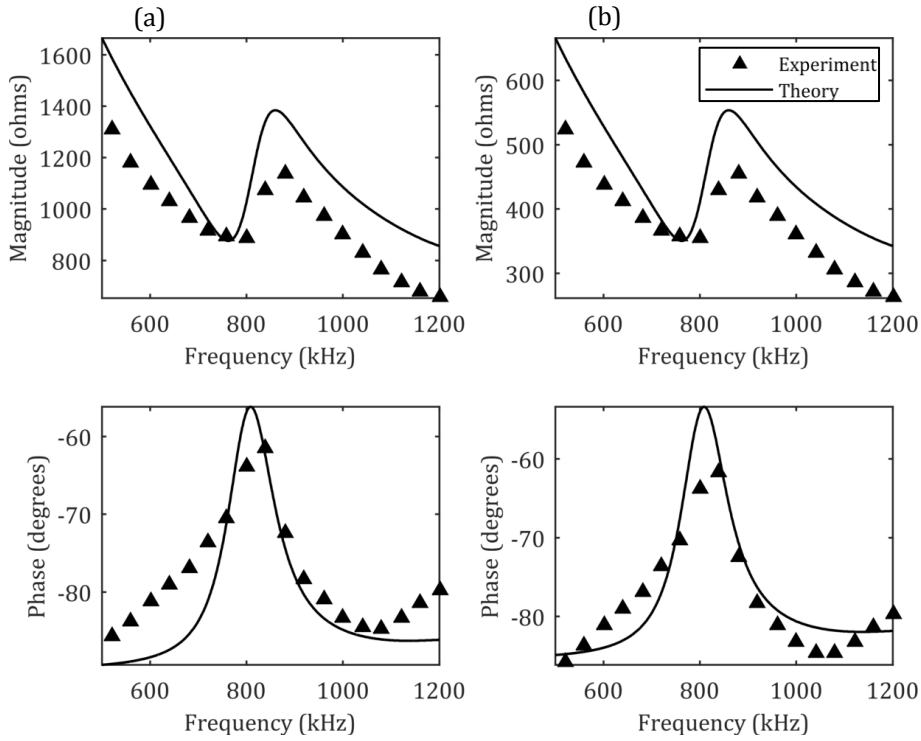

Figure 7. Theoretical and experimental electrical impedance. (a) Single element #53. (b) Element pair #53.

At this stage, the electrical impedance of the association is significantly changed – the complex impedance decreases and becomes entirely real near the resonance. The impedance magnitude is around 100 Ω and the transducer operates with maximized efficiency. The inductive load alters the resonance frequency of the element pair, which is slightly shifted to the left. This may not cause significant changes in the transducer operation.

Figure 9 shows the pulse-echo time-domain response and its fast Fourier transform (FFT) of a single element, and an element pair with and without inductor network when driven by one cycle of 100 V_{pp} short duration (2 µs) square wave pulse. For this purpose, it was used an ultrasonic pulser/receiver unit (5077PR, Panametrics-NDT) and a brass block reflector placed at 50 mm distant from the transducer. An echo of almost 6 V_{pp} and a broad bandwidth were observed after the insertion of inductor network. This response provided means to calculate the two-way insertion loss of each element configuration.

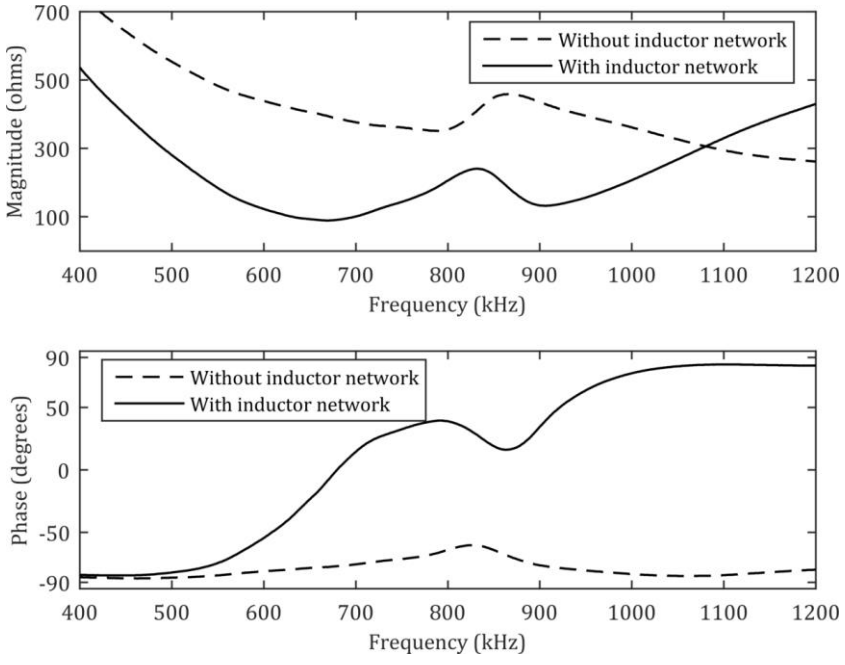

Figure 8. Electrical impedance of element pair #53 with and without the series tuning inductor network.

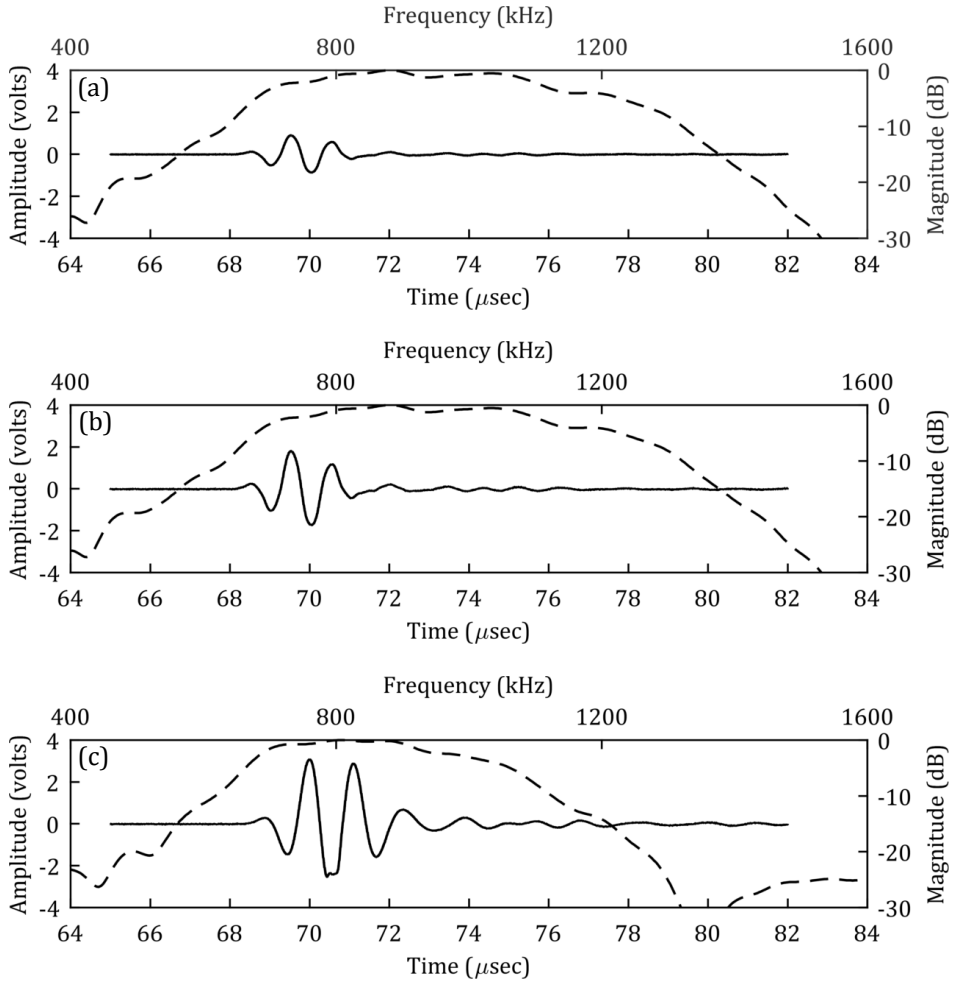

Figure 9. Time (solid line) and frequency-domain (dashed line) pulse-echo responses. (a) Single element #56. (b) Element pair #56. (c) Element pair #56 with inductor network.

The simulated and measured acoustic field of an element pair with inductor network are shown in Fig. 10. The simulation agrees well in radiation pattern with the measurement result. The transducer was precisely aligned in the three dimensions within the water tank to produce a radiation pattern that is symmetrical in relation to the *x* direction.

The overall performance of each element configuration is summarized in Table 2. Evidently, the approach herein proposed to the array arrangement provided a significant improvement in the power transfer efficiency of the fabricated transducer array. It is plausible that the two-way insertion loss for an element pair with inductor network is 10 dB less than for a configuration with a single element.

A photograph of the completed 2D ultrasound transducer array is shown in Fig. 11.

Table 2. Averaged experimental results for a single element, element pair and element pair with inductor network.

Configuration	Center frequency (kHz)	Clamped capacitance (pF) [(1)]	Impedance magnitude (Ω) [(1)]	Impedance phase (°) [(1)]	-6 dB bandwidth (%)	Insertion loss (dB) [(1)]
Single element	961.15	254	803	-71	60.93	35.86
Element pair	962	560	365	-69	60.97	29.02
Element pair with inductor network	866	–	81	-1	49.31	25.11

[(1)] measured at resonant frequency

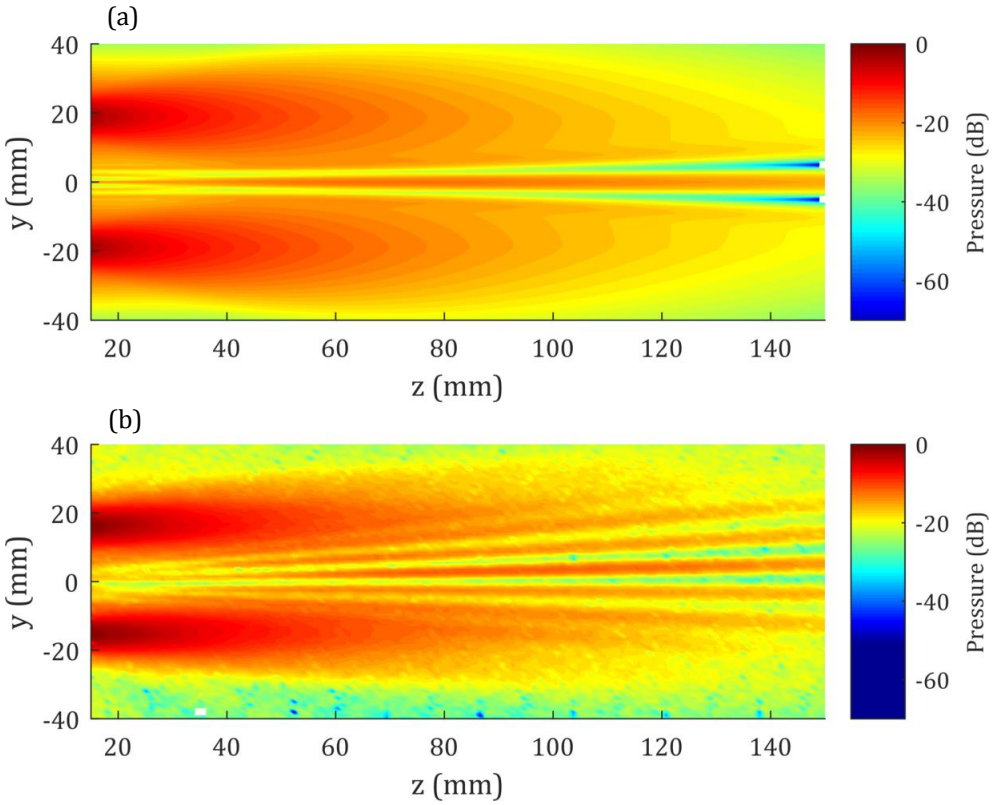

Figure 10. Acoustic field of element pair #58 with inductor network. (a) Simulated. (b) Measured.

Figure 11. A picture of the finished ultrasound transducer probe.

5. CONCLUSION

The design of a 2D array transducers presents many technical challenges due to the large number of elements with a very small cross-sectional area. Prior works have investigated methods to improve transmit efficiency of these transducers, however, since these studies involve transducers for image generation, they do not always guarantee the maximum efficiency for ARFI excitation.

In this work, we proposed an array arrangement that is capable of reducing both the number of necessary driving channels and the electrical impedance of the transducer. The fabricated transducer array presented a high transmit efficiency, broad bandwidth and insertion loss of 10 dB less when compared to a conventional transducer. Our results suggest that this approach of array arrangement appears to have potential to be applied in the design of constantly focused transducers for ARFI imaging. Considering that it was not possible to simultaneously drive all 128 array elements of the fabricated transducer, future work should include the experimental measurement of its focusing and steering properties.

6. ACKNOWLEDGEMENTS

This work was supported by CAPES Foundation. We are grateful for the contribution of many people in the Laboratory of Ultrasound at the School of Engineering of the University of Sao Paulo.

7. REFERENCES

Benson, J. & Fan, L., 2012. "Tissue Strain Analytics - A Complete Ultrasound Solution for Elastography". *White Paper Siemens Medical Solutions*, December, pp. 1-20.

Bronzino, J. D., 2000. *The Biomedical Engineering HandBook.* 2nd ed. Boca Raton(FL): CRC Press LLC.

Cardoso, F. M., Santos, D. S. & Furuie, S. S., 2016. "Acoustic Radiation Force Impulse In Deep Tissues Using Matricial Array Transducers". *Congresso Brasileiro de Engenharia Biomédica - CBEB 2016*, pp. 1075-1078.

Desilets, C. S., Fraser, J. D. & Kino, G. S., 1978. "The Design of Efficient Broad-Band Piezoelectric Transducers. *IEEE Trans. Sonics Ultrason".*, May, SU-25(3), pp. 115-125.

DeWall, R. J., 2013. "Ultrasound Elastography: Principles, Techniques, and Clinical Applications". *Critical Reviews™ in Biomedical Engineering*, 41(1), pp. 1-19.

Doherty, J., Trahey, G., Nightingale, K. & Palmeri, M., 2013. "Acoustic radiation force elasticity imaging in diagnostic ultrasound". *IEEE Trans. Ultrason. Ferroelectr. Freq. Control*, 60(4), pp. 685-701.

Goldberg, R. L. & Smith, S. W., 1994. "Multilayer Piezoelectric Ceramics for Two-Dimensional Array Transducers". *IEEE Trans Ultrason Ferroelectr Freq Control*, September, 4(5), pp. 761-771.

Hunt, J. W., Arditi, M. & Foster, F. S., 1983. "Ultrasound Transducers for Pulse-Echo Medical Imaging". *IEEE Transactions on Biomedical Engineering*, August, BME-30(8).

Kino, G. S., 1987. *Acoustic Waves: Devices, Imaging, and Analog Signal Processing.* Englewood Cliffs(NJ): Prentice-Hall.

Kinsler, L. E. & Frey, P., 1962. *Fundamentals of Acoustics.* New York: John Wiley & Sons.

Krimholtz, R., Leedom, D. A. & Matthaei, G. L., 1970. "New equivalent circuits for elementary piezoelectric transducers". *Electronics Letters*, June, 6(13), pp. 398-399.

Nightingale, K., 2012. "Acoustic Radiation Force Impulse (ARFI) Imaging: a Review". *Curr. Med. Imaging Rev.*, 7(4), p. 328–339.

Oliveira, T. F. d., 2015. *Transdutores de ultrassom multielementos lineares flexíveis com sensor de curvatura para superfícies curvas. Doctoral Thesis,* University of São Paulo, São Paulo, Brazil.

Ophir, J. et al., 1996. "Elastography: ultrasonic imaging of tissue strain and elastic modulus in vivo". *European Journal of Ultrasound* , Volume 3, pp. 49-70.

Sarvazyan, A. et al., 2012. "An Overview of Elastography – An Emerging Branch of Medical Imaging". *Curr. Med. Imaging Rev.*, November, 7(4), p. 255–282.

Sarvazyan, A. P. et al., 1995. "Biophysical Bases of Elasticity Imaging". *Acoustical Imaging*, January, Volume 21, pp. 223-240.

Shung, K. K. & Zipparo, M. J., 1996. "Ultrasonic Transducers and Arrays". *IEEE Engineering in Medicine and Biology*, November, 15(6), pp. 20-30.

Szabo, T. L., 2004. *Diagnostic Ultrasound Imaging: Inside Out.* Newburyport, MA, USA: Elsevier Academic Press.

Turnbull, D. H. & Foster, F. S., 1991. "'Beam Steering with Pulsed Two-Dimensional Transducer Arrays". *IEEE Trans Ultrason Ferroelectr Freq Control*, July, 39(4).

Turnbull, D. H. & Foster, F. S., 1992. "Fabrication and Characterization of Transducer Elements in Two-Dimensional Arrays for Medical Ultrasound Imaging". *IEEE Trans Ultrason Ferroelectr Freq Control*, July, 39(4), pp. 464-475.

Zhou, Q. et al., 2014. "Piezoelectric single crystals for ultrasonic transducers in biomedical applications". *Prog Mater Sci.*, October, Volume 66, p. 87–111.

8. RESPONSIBILITY NOTICE

The authors are the only responsible for the printed material included in this paper.